Korean J. Chem. Eng., 34(1), 73-80 (2017)
DOI: 10.1007/s11814-016-0248-6

pISSN: 0256-1115
eISSN: 1975-7220

Photocatalytic degradation of toluene in a staged fluidized bed reactor using TiO_2/silica gel

Hsiu-Po Kuo*,,†, Shang-Wen Yao*, An-Ni Huang*,***, and Wan-Yi Hsu***

*Department of Chemical and Materials Engineering, Chang Gung University, Taoyuan 33302, Taiwan
**Department of Otorhinolaryngology, Chang Gung Memorial Hospital, Linkou, Taoyuan 33305, Taiwan
***Department of Chemical Engineering, Graduate School of Engineering, Hiroshima University, Hiroshima 739-8527, Japan
(*Received 16 May 2016 • accepted 29 August 2016*)

Abstract−Relatively high concentration toluene is photocatalytically degraded in a multi-stage fluidized bed reactor continuously. The fluidizing media are titanium dioxide deposited silica gel particles, which are prepared by the doping sol-gel method. The effects of the Ti/Si atomic ratio, the inlet gas flow rates, and the number of the stages on the toluene removal efficiency were evaluated. The highest toluene removal efficiency is obtained when the fluidizing media are with the Ti/Si atomic ratio of 1.25. The apparent reaction orders are 0.4-0.5 for the single-stage system and 0.7 for the two-stage system, respectively. With an inlet toluene concentration of 1,000 ppm, a relative humidity of 30% and a volumetric flow rate of 10 L/min, the removal efficiency of toluene at the steady state is as high as 80% and is maintained in the 6-hr experimental time.

Keywords: Fluidized Bed, Multi-stage, Toluene, Photocatalytic Degradation

INTRODUCTION

Titanium dioxide, TiO_2, showing relatively high catalytic activity under UV irradiation has been widely used in environmental applications [1]. Volatile organic compounds (VOC) photocatalytic degradation by TiO_2 under UV irradiation is probably one of the most widely studied topics in these applications [2,3]. Acetone, cyclohexane, methyl ethyl ketone, toluene, phenol and other VOCs have been successfully degraded by TiO_2 under light irradiation [4-7]. The reaction pathways have also been comprehensively studied [8,9]. The hole-electron pairs are formed when TiO_2 is under light irradiation. The hole-electron pairs react with water, oxygen, and/or other substances and subsequently produce active free radicals, which effectively degrade the VOCs. Although photocatalytic degradation of VOC by TiO_2 under light irradiation has been extensively studied, these studies typically use VOC with relatively low concentrations. The reaction space time was relatively long and the throughput was relatively low. Continuous degradation of relatively high concentration VOC (say hundreds ppm) by TiO_2 under light irradiation remains challenging.

VOC photocatalytic degradation by TiO_2 is a heterogeneous reaction. VOC molecules mass transferring from the bulk to the TiO_2 surfaces are then oxidized by the active free radicals. Except for special cases, the concentration of VOC in the bulk is usually relatively low and the thermodynamic constraint further limits VOC molecule absorption onto the TiO_2 surfaces. Several attempts have been proposed to enhance the VOC mass transferring from bulk to the TiO_2 surfaces. The concentration of VOC has been enriched by the porous sorbents and the increasing of the concentration gradient between the porous sorbents and TiO_2 enhanced VOC mass transferring to the TiO_2 surfaces. Based on this terminology, TiO_2 particles had been immobilized on different porous sorbent, includes activated carbon, γ-Al_2O_3, silica, zeolite and ceramic foam particles [2,4,6,7,10-12].

Another approach to enhance VOC mass transferring is by using fluidized bed photoreactors. Fluidized bed photoreactors provide massive contact areas between gaseous VOC and solid TiO_2 particles and are ideal for heterogeneous VOC degradation reactions [7,13,14]. TiO_2 powder immobilized porous sorbents have been used as the fluidizing media. Immobilization not only enriches the local VOC concentrations near TiO_2 powders, but also reduces TiO_2 powder elutriation. Nevertheless, particle collisions are usually significant in a fluidized bed reactor and porous sorbents (for example, activated carbons) may be broken.

Porous silica gels are often used in petrochemical industries for absorption or as the packing materials in chromatography. Silica gels are commercially available products which are readily available to use and show good wearing properties. TiO_2 was immobilized on porous silica gels by the doping sol-gel method in this work. The physical and chemical properties of these particles were characterized. The as-prepared particles were used as the fluidizing media in a fluidized bed photoreactor for continuous high concentration toluene vapor degradation. The effects of the Ti/Si atomic ratio, the inlet gas flow rates, and the number of the stages on the toluene removal efficiency were studied.

EXPERIMENTAL METHOD

Spherical silica gels with the mean size of 90 μm are used as the support of the fluidizing material (CHROMATOREX®-MB70, Fuji

†To whom correspondence should be addressed.
E-mail: hpkuo@mail.cgu.edu.tw

Table 1. The formulas for TiO_2/SiO_2 particle preparation

TiO_2/SiO_2	TTIP [g]	Ethanol (A+B) [ml]	Silica gel [g]
T_3S_4	10	65	5
T_5S_4	30	135	5
T_9S_4	30	135	2

Silysia Chemical, Japan). The density and the surface area of the silica gel particles are 500.0 kg/m^3 and 525.14 m^2/g, respectively. Silica gels supported TiO_2 particles (TiO_2/SiO_2) were prepared by doping silica gel particles during the preparation of TiO_2 by the sol-gel method. The details are as follows.

Ttitanium isopropoxide (TTIP, Acros organic) was stirred with anhydrous ethanol for 5 min. Silica gel particles were added into the TTIP/anhydrous ethanol mixture together with 125 µl nitric acid (J.T.Baker). This mixture was named solution A. Solution B was a mixture of 7 ml de-ion water and 15 ml anhydrous ethanol. Solution A and solution B were gently mixed and gelled. The gel was then sealed in a jar and aged at room temperature for three days. The aged gel was dried in a 100 °C oven for 24 h. The TiO_2/SiO_2 particles were thereby obtained after 4-hr 450 °C calcination.

Three formulas were designed to prepare TiO_2/SiO_2 particles with different Ti/Si atomic ratios. Table 1 summarizes the formulas. T_xS_y indicates the Ti/Si atomic ratio of TiO_2/SiO_2 determined by energy dispersive spectroscopy (EDS, model 6587, Oxford Instrument). The properties of the TiO_2/SiO_2 particles were further characterized. The morphology of the TiO_2/SiO_2 particles was observed by scanning electron microscope (SEM, SNE-4500M). The BET specific surface area of TiO_2/SiO_2 particles was measured by high purity nitrogen adsorption (ASAP 2020, Micromeritics). The crystalline of the TiO_2/SiO_2 particles was characterized by X-ray diffraction (XRD, D5005D, Siemens). The band-gap energies of these samples were determined by a UV-Vis spectrophotometer (V-650, JASCO). The chemical bonding of TiO_2/SiO_2 particles was analyzed by X-ray photoelectron spectroscopy (XPS, Theta Probe, Thermo Scientific).

The prepared TiO_2/SiO_2 particles were used as the fluidized media in a specially designed fluidized bed photoreactor. A schematic drawing of the system is shown in Fig. 1(a). High pressure air was stored in the tank (a). Air was dried by the dryer (b) after leaving the tank (a). An air mass flow controller (c) was used to control the flow rate of the air stream. The concentration of toluene and the humidity of the inlet stream were controlled by the toluene evaporator (e) and the water evaporator (f), respectively. The cylindrical fluidized bed reactor (j) was made of quartz with an internal diameter of 5 cm. A UV light tube (i) was inserted at the center of the fluidized bed reactor (j).

The design of the reactor is shown in Fig. 1(b). The reactor consists of five shorter cylindrical columns. The cylindrical columns were connected by the flanges and clamps. Screen printing cloths (mesh number 200) were placed between the cylindrical columns. The gas distributor at the bottom of the reactor is a stainless steel support covered by a screen printing cloth with a mesh number of 200. The 15 W UV light has an outer diameter of 2.1 cm. The wavelength of the light is 254 nm. The toluene concentrations of the gas stream before and after the photocatalytic degradation reaction were determined by gas chromatograph (Autosystem XL, PerkinElmer).

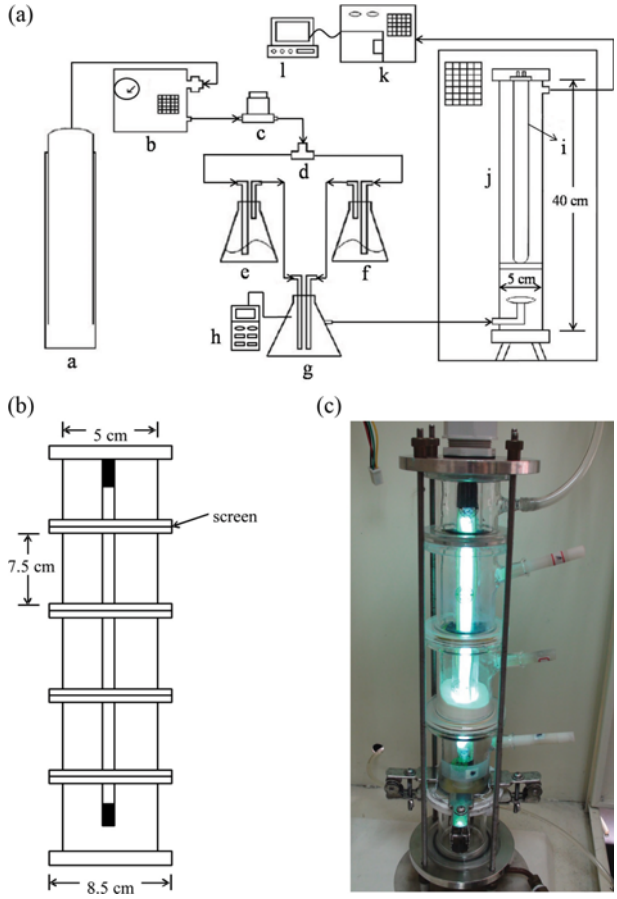

Fig. 1. (a) Schematic diagram of the experimental system. a: Air storage tank; b: Dryer; c: Mass flow controller; d: Three-way valve; e: Toluene evaporator; f: Water evaporator; g: Mixer; h: Humidity meter; i: UV light; j: Fluidized bed reactor; k: GC; *l*: PC. (b) The enlargement of the fluidized bed reactor. (c) A photo of the fluidized bed reactor.

A photo of the reactor with the UV lamp is shown in Fig. 1(c).

In a typical experiment, TiO_2/SiO_2 particles were loaded into the reactor as the fluidizing media. In the single-stage experiment, 20.0 g of the fluidizing media was loaded into the lowest cylindrical column. In the two-stage experiment, a total amount of 40.0 g fluidizing media was loaded in the lowest two cylindrical columns (20.0 g each). The relative humidity of the inlet stream was controlled at 30±2%. The inlet stream volumetric flow rate, F, was set at 5 L/min, 10 L/min or 15 L/min. The toluene concentration of the inlet stream, C, was set at 300 ppm, 650 ppm or 1,000 ppm. Toluene removal efficiency is defined as,

$$\text{Toluene removal efficiency (\%)} = \frac{\text{inlet toluene concentration} - \text{outlet toluene concentration}}{\text{inlet toluene concentration}} \times 100\%$$

RESULTS AND DISCUSSION

1. TiO_2/SiO_2 Particle Characterization

The morphologies of the TiO_2/SiO_2 particles together with the

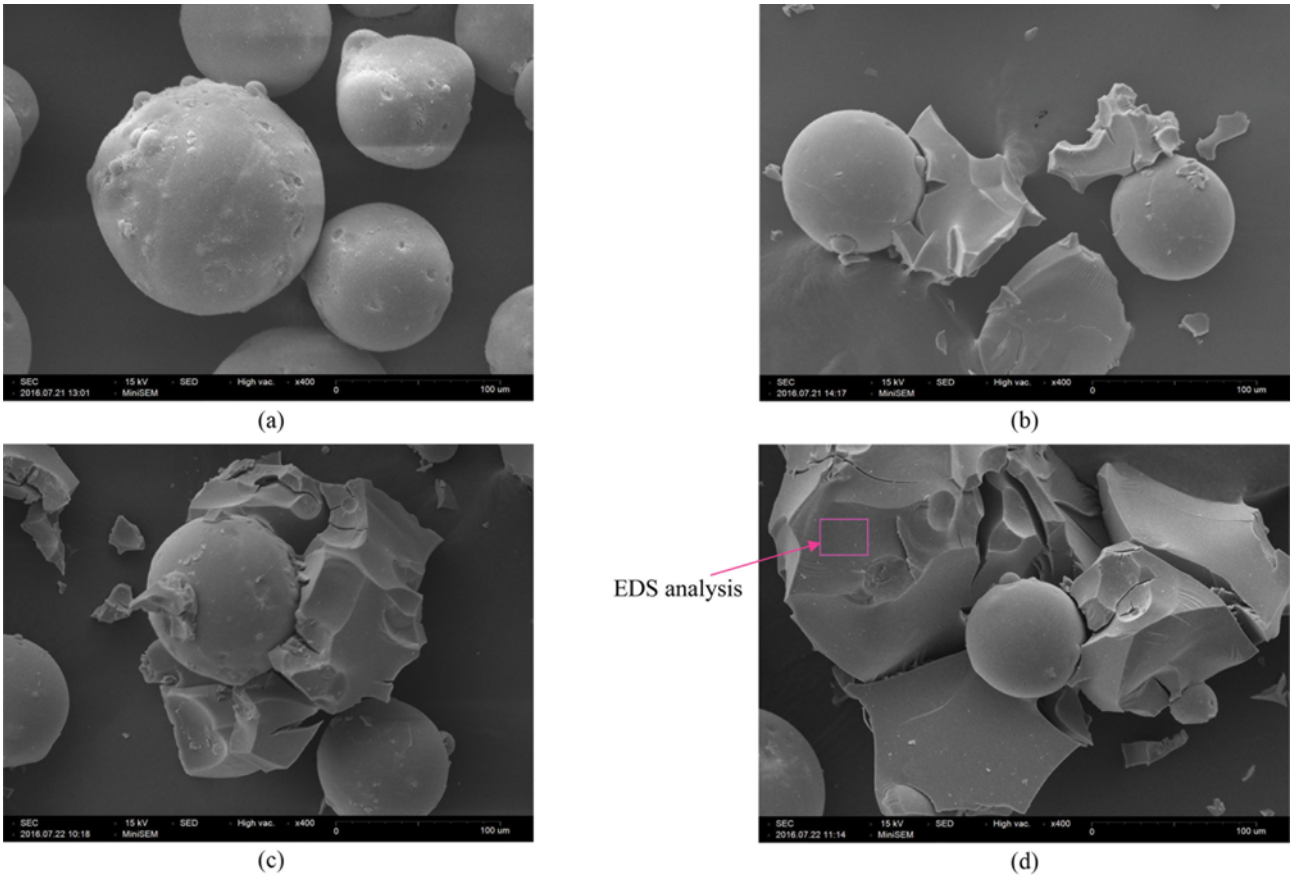

Fig. 2. SEM images of (a) silica gel, (b) T_3S_4, (c) T_5S_4, and (d) T_9S_4 particles.

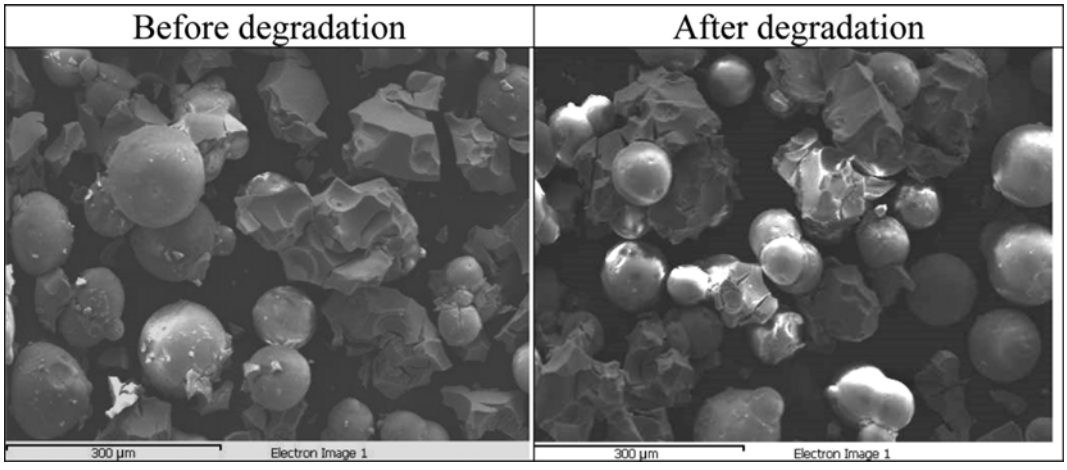

Fig. 3. SEM images of T_5S_4 particles before and after the toluene fluidization degradation operations.

original silica gel particles are realized by the SEM images in Fig. 2. Flaky materials are observed on the spherical silica gel particles. The amount of the flaky materials increases with the increasing of the Ti/Si atomic ratio. The flaky materials in Fig. 2 were analyzed by EDS. The atomic ratio of Ti : Si : O is 33.87 : 0.32 : 65.81. The flaky material is mainly TiO_2 from EDS analyses.

One of the major concerns of using TiO_2/SiO_2 particles in the fluidized bed photoreactors as the fluidizing media is the attrition of the TiO_2/SiO_2 particles. The flaky TiO_2 deposited on the silica gel particles may be lost after the fluidization operation if attrition is severe. The SEM images of T_5S_4 particles before and after the fluidized bed toluene degradation reactions are shown in Fig. 3 (F=10 L/min; C=300 ppm). The flaky TiO_2 remains deposited on the spherical silica gel particle surfaces after 6-hr fluidization experimental run. The results in Fig. 3 indicate that the TiO_2/SiO_2 particles prepared by the doping sol-gel method show good wearing properties.

Table 2. Density, BET specific surface area and band gap energy of TiO_2/SiO_2 particles

TiO_2/SiO_2	Density (kg/m^3)	BET before calcination (m^2/g)	BET after calcination (m^2/g)	Band gap energy (eV)
T_3S_4	2570	559.51	390.50	3.10
T_5S_4	2810	403.26	225.93	2.94
T_9S_4	3240	326.19	148.87	2.92

Table 3. The comparisons of the equilibrium toluene removal efficiencies (ERE) and the apparent reaction rate constant (k) and order (n) at different operation conditions

F (L/min)		5				10				15			
		Stages											
	Toluene concentration (ppm)	1		2		1		2		1		2	
		ERE	k (ppm/s-L) n	ERE	k (ppm/s-L) n	ERE	k (ppm/s-L) n	ERE	k (ppm/s-L) n	ERE	k (ppm/s-L) n	ERE	k (ppm/s-L) n
T_3S_4	300	51	8.3	76	2.7	55	22.3	80	6.1	45	21.5	78	10.7
	650	39		72		44		77		33		75	
	1000	30	0.5	69	0.7	32	0.4	74	0.7	26	0.5	72	0.7
T_5S_4	300	57	15.8	81	3.6	62	33.9	87	13.4	53	29.1	84	13.9
	650	46		78		51		84		40		81	
	1000	32	0.4	74	0.7	37	0.4	80	0.7	32	0.5	77	0.7
T_9S_4	300	39	3.1	77	2.7	42	8.2	81	6.1	52	27.6	85	13.3
	650	32		73		34		79		42		82	
	1000	26	0.5	69	0.7	28	0.5	75	0.7	32	0.5	79	0.7

The density, BET specific surface area and band gap energy of TiO_2/SiO_2 particles are summarized in Table 3. Since atomic mass of Ti is much larger than that of Si, the density of TiO_2/SiO_2 particles increases when the Ti/Si atomic ratio increases. The minimum fluidization velocity of the particles was calculated by the correlations of Geldart [15]. The minimum fluidization velocities, U_{mf}, of T_3S_4, T_5S_4 and T_9S_4 were 0.0046 m/s, 0.0051 m/s and 0.0058 m/s, respectively. The tested volumetric flow rates (7.3-27.7 U_{mf}) are well above the of the minimum fluidization velocities of the corresponding T_xS_y TiO_2/SiO_2 particles to ensure the fluidization of the bed. The band-gap energies of these samples were determined by the UV-Vis spectrophotometer. The band gaps of T_3S_4, T_5S_4, T_9S_4 were determined and shown in Table 2 as 3.10 eV, 2.94 eV and 2.92 eV, respectively. For reference, the band gap is 3.0 eV for rutile TiO_2 and 3.2 eV for anatase TiO_2. The band gap narrows with the increasing of the Ti/Si atomic ratio and particles with higher Ti/Si atomic ratio show better photodegradation activity [16].

The BET specific surface area of the original silica gel particles was 525.14 m^2/g. Before calcination, T_3S_4 had a larger BET specific surface area than that of the original silica gel particles. A relatively small amount of sol-gelled particles on the silica gel particle surface increases the BET specific surface areas of the mother particles. However, when the Ti/Si atomic ratio increases to 5/4 or 9/4, the addition of sol-gelled particles fills into the pores of silica gel particles. The blockage of the pores causes the decreasing of the BET specific surface area of T_5S_4 or T_9S_4 mother particles before calcination. It is interesting that the BET specific surface area of all TiO_2/SiO_2 particles decreases after calcination. The formation of the flaky

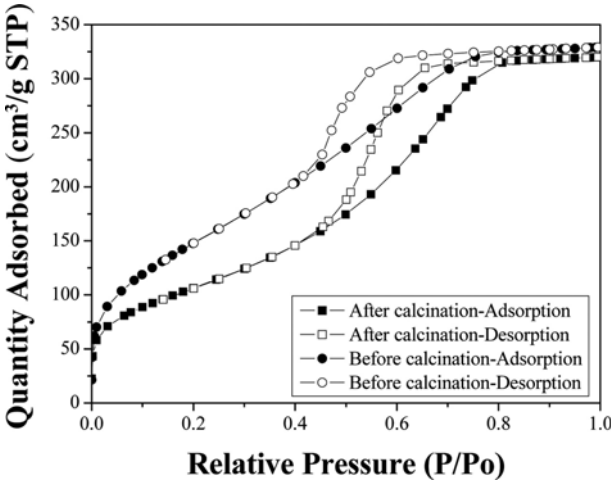

Fig. 4. The absorption and desorption isotherms of T_3S_4 particles before and after calcination.

TiO_2 on the mother particle surfaces covers the silica gel particle pores. The absorption isotherms of the T_3S_4 particles before and after calcinations are shown in Fig. 4. The amount of the adsorbed nitrogen molecules was reduced after calcinations due to the coverage of the silica gel pores by TiO_2. The results in Fig. 4 indicate that these particles have Type IV isotherm with mesopores in the range of 2 nm to 50 nm [17].

The XRD analyses of the TiO_2/SiO_2 particles before and after calcinations are shown in Fig. 5. It is confirmed that the formation

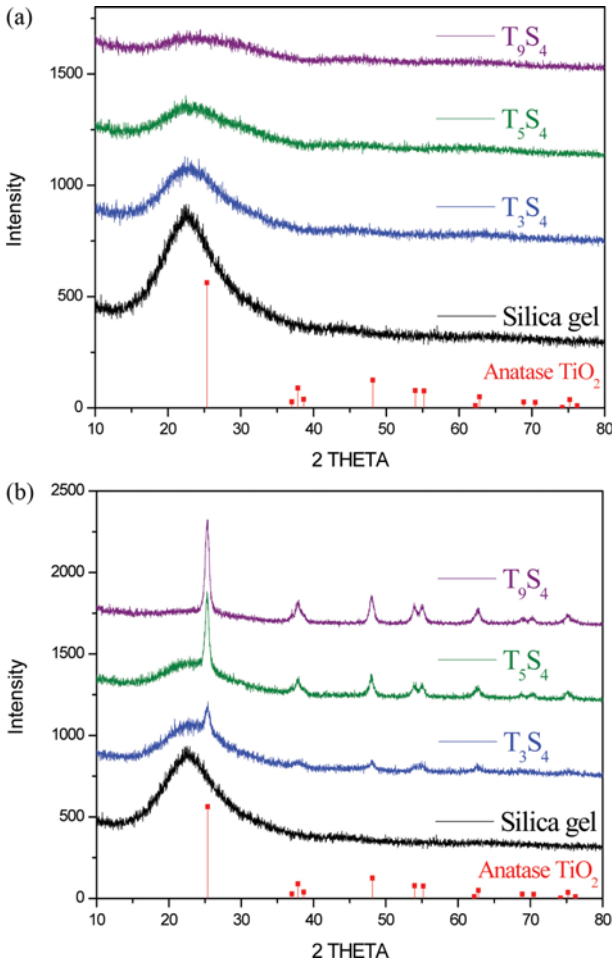

Fig. 5. XRD spectra of TiO_2/SiO_2 particles (a) before and (b) after calcinations.

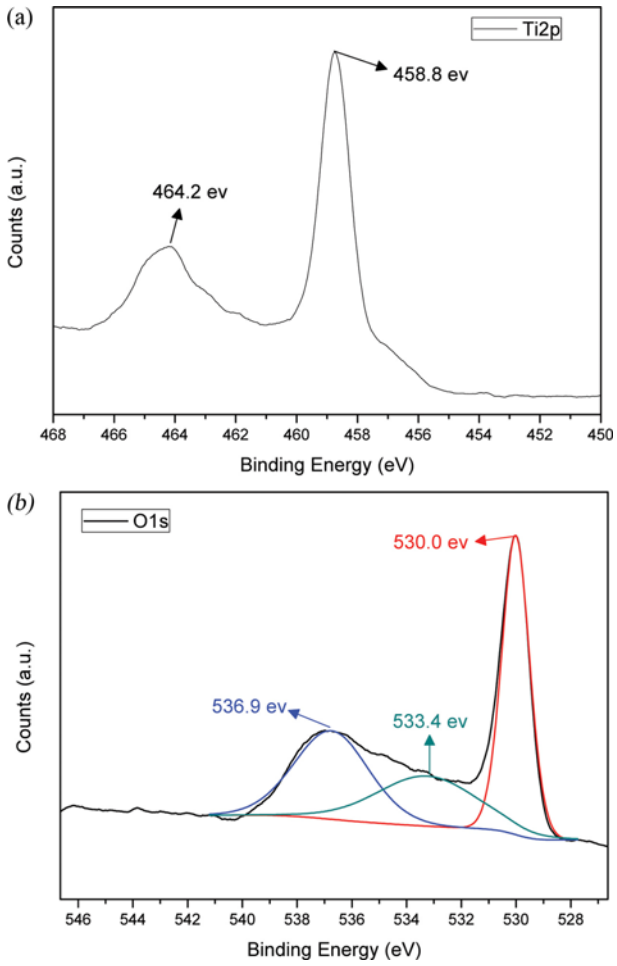

Fig. 6. XPS spectra of T_9S_4 particles: (a) spectrum of Ti 2p; (b) spectrum of O 1s.

of anatase TiO_2 after calcination causes particle densification and the decreasing of the BET specific surface area. The XRD peaks reveal trace amount of silica gel after calcination, especially in the case of T_9S_4. The suppressed silica gel peaks partially result from the TiO_2 coating shells. XPS was used to further investigate the chemical states of Ti and O in silica gel XRD peak suppressed T_9S_4 particles. Fig. 6(a) shows the XPS spectra for Ti 2p. Ti $2p_{1/2}$ and Ti $2p_{3/2}$ of T_9S_4 appear at 464.2 eV and 458.8 eV, respectively, indicating that Ti exists in the form of Ti^{4+} [18]. The binding energy of Ti $2p_{3/2}$ for T_9S_4 is 0.6 eV greater than that of pure TiO_2 of 458.2 eV [19]. The formation of Si-O-Ti bond can cause a 0.6 eV increasing of the binding energy of Ti $2p_{3/2}$ and Si-O-Ti bond enhances the photocatalytic activity of the fluidized media [16]. Fig. 6(b) shows the O 1s XPS spectrum. The peaks were predominantly fitted into three peaks, which correspond to 530.0 eV, 533.4 eV and 536.9 eV. The binding energies of O 1s in Ti-O-Ti and Si-O-Si and bonds are 530.1 eV and 533.2 eV, respectively [17]. A binding energy of 536.9 eV in O 1s spectrum refers to some unspecified metal oxide, possibly Si-O-Ti.

2. Toluene Degradation

Figs. 7, 8 and 9 show the comparisons of the toluene removal efficiencies in the single-stage and two-stage degradation systems with different inlet toluene concentrations and inlet gas volumetric flow rates using T_3S_4, T_5S_4 and T_9S_4 particles as the fluidizing media, respectively. In all cases, the toluene removal efficiency drops quickly in the first 20-25 min in the single-stage systems and remains an almost constant value in the reaction time studied. The constant value is referred to as the equilibrium toluene removal efficiency. The toluene removal efficiency drops are much later in the two-stage systems. When the inlet toluene concentration increases, the equilibrium toluene removal efficiency decreases.

There are two mechanisms involving the removal of toluene from the gaseous stream: silica gel absorption removal and TiO_2 photocatalytic degradation. The removal of toluene from the gas stream via the relative fast silica gel absorption is effective in the first period and toluene removal efficiency is nearly 100% (for example, first 50 min in the two-stage systems). However, when the toluene absorption on silica gel reaches equilibrium, toluene is not able to be removed by the silica gel absorption mechanism and the toluene removal efficiency keeps decreasing. A reference experimental run was carried out using pure silica gel as the fluidizing media, the toluene removal efficiency gradually decreases and does not reach an equilibrium toluene removal efficiency. In the single-stage degradation experiments, the total amount of the silica gel loaded in

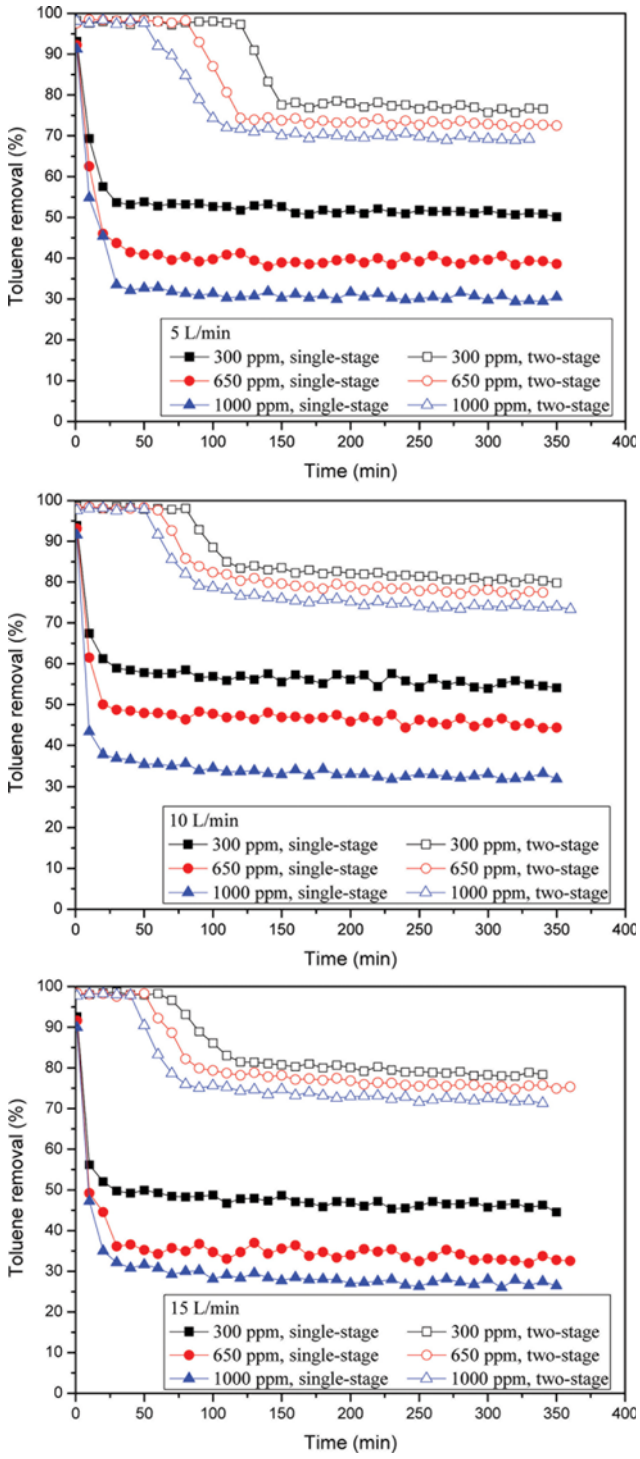

Fig. 7. The comparisons of the toluene removal efficiencies of the single-stage and two-stage systems operated at different operation conditions and using T_3S_4 particles as the fluidizing media.

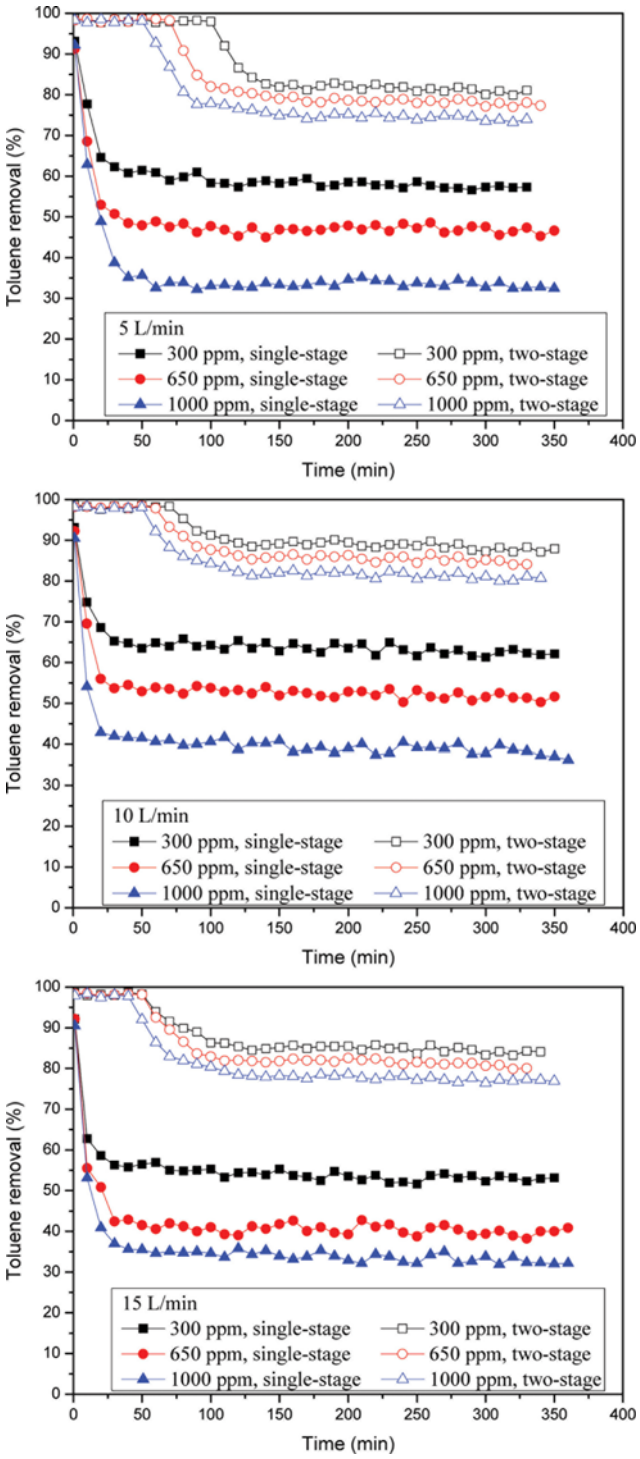

Fig. 8. The comparisons of the toluene removal efficiencies of the single-stage and two-stage systems operated at different operation conditions and using T_5S_4 particles as the fluidizing media.

the system is limited and the loaded silica gels are not able to remove the entire toluene from the gas stream. The toluene removal efficiency drops quickly and a near 100% removal efficiency in the first period is too short to be observed in the single-stage experiments. In the two-stage experiments, the total amount of silica gels is large enough to show a near 100% removal efficiency in the first period. The removal efficiency of toluene from the gas stream drops after the toluene absorption reaching equilibrium. The TiO_2 photocatalytic toluene degradation mechanism dominates in the second period and toluene removal efficiency profile follows that in

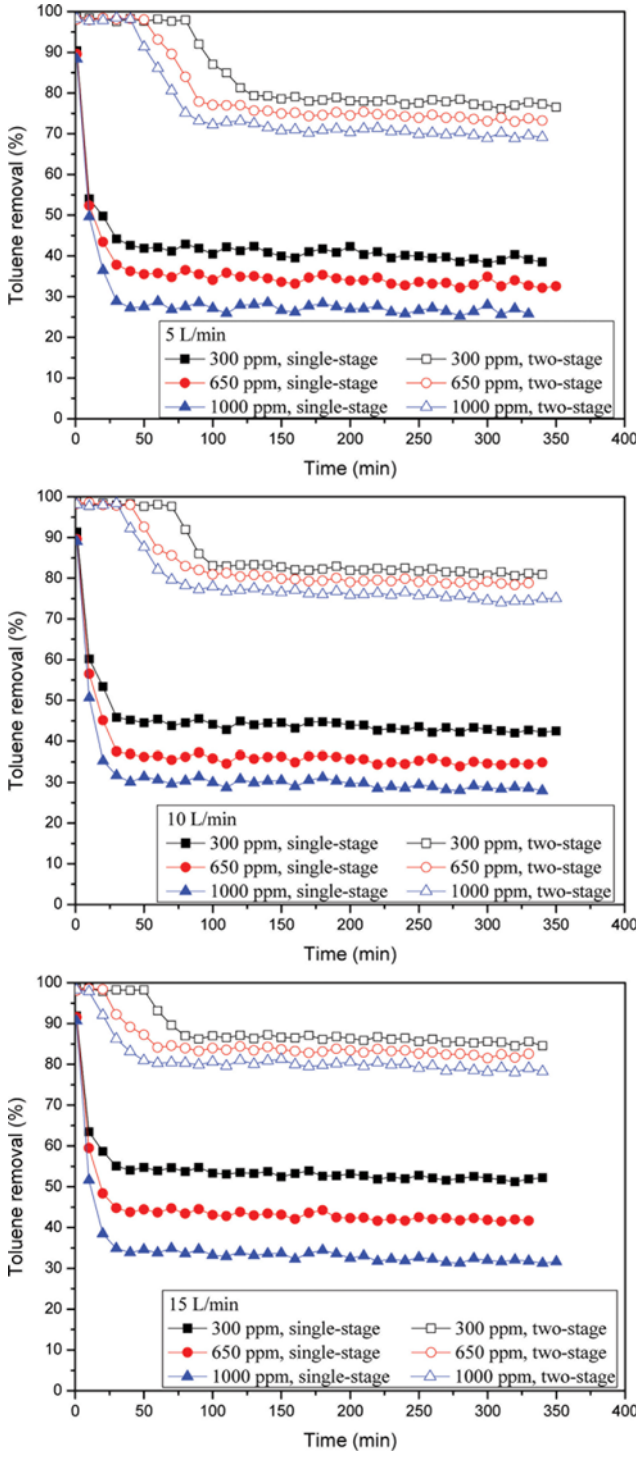

Fig. 9. The comparisons of the toluene removal efficiencies of the single-stage and two-stage systems operated at different operation conditions and using T_9S_4 particles as the fluidizing media.

the single-stage experiments. If the toluene mass transferring from the bulk to the particle surface is *not* the rate limiting step, the results indicate that the number of the active sites of the TiO_2/SiO_2 particles is not large enough to degrade the toluene molecules in the inlet stream when the inlet toluene concentration increases. Since

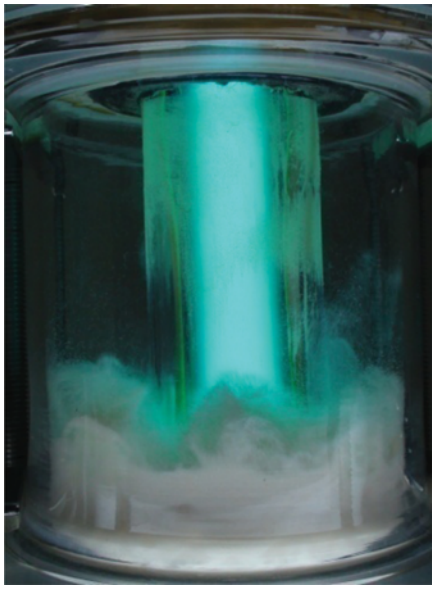

Fig. 10. A slug flow regime in the single-stage system using T_5S_4 particles as the fluidizing media (F=10 L/min).

the high concentration toluene is continuously fed into the system and the steady state operation is achieved after 20-25 min in the single-stage systems. Continuous toluene degradation operation is successfully achieved.

The inlet gas volumetric flow rate, *F*, affects the fluidized bed flow regimes and the toluene residence time and thus the equilibrium toluene removal efficiency. Theoretically, a small F value allows the toluene vapor to have a longer residence time and thus higher toluene removal efficiency. However, the inlet gas volumetric flow rate also affects the bed flow regime. In the parameters studied, a packing bed, a bubbling fluidized bed, a slug fluidized bed or a turbulent fluidized bed may exist. Among these beds, a slug fluidized bed is preferred for toluene photocatalytic degradation. A slug fluidized bed allows good contact between TiO_2/SiO_2 particles and toluene molecules and the large bubbles in the bed allow UV light deep penetration. An example of slug fluidized bed is shown in Fig. 10 when using T_5S_4 as the fluidizing media.

In the single-stage system, a bubbling fluidized bed is obtained at *F*=5 L/min using T_3S_4 or T_5S_4 as the fluidizing media and a slug fluidized bed is obtained at *F*=10 L/min using T_3S_4 or T_5S_4 as the fluidizing media. A turbulent fluidized bed is obtained at *F*=15 L/min using T_3S_4 or T_5S_4 as the fluidizing media. When using the relative light T_3S_4 or T_5S_4 as the fluidizing media, the equilibrium toluene removal efficiency is the highest at *F*=10 L/min and the bed shows a slug flow regime. In the inlet gas flow rates studied, there are no slug flow regimes when using T_9S_4 as the fluidizing media. T_9S_4 has the highest density and a bubbling fluidized bed is obtained at *F*=15 L/min. When using relatively heaver T_9S_4 as the fluidizing media, the equilibrium toluene removal efficiency is the highest at *F*=15 L/min. The equilibrium toluene removal efficiency is also affected by dual effects of the gas residence time and the flow regimes in the two-stage systems. The equilibrium toluene removal efficiency is the highest at *F*=10 L/min using T_3S_4 or T_5S_4 as the fluidizing media or at *F*=15 L/min using T_9S_4 as the fluidizing media.

A higher equilibrium toluene removal efficiency of 87% is obtained in the two-stage system using T_5S_4 as the fluidizing media with an inlet toluene concentration of 300 ppm and inlet flow rate of 10 L/min.

The comparisons of the equilibrium toluene removal efficiency in the single-stage systems and that in the two-stage systems are shown in Table 3. The equilibrium toluene removal efficiency in the two-stage system is generally higher than that in the single-stage system. The apparent reaction rate constant and order were determined by inlet toluene concentrations and toluene equilibrium concentrations using the CSTR model at different operating conditions. The results are also summarized in Table 3. The apparent reaction orders are 0.4-0.5 for single-stage reactors and 0.7 for two-stage reactors, respectively. The coupling effects of particle photodegradation activity and the hydrodynamic behavior cause higher apparent reaction rate constants when using T_5S_4 particles as the fluidizing media. The highest toluene removal efficiency of 87% was obtained in the two-stage system when using T_5S_4 as the fluidizing media at the inlet toluene concentration of 300 ppm and F=10 L/min. When the inlet concentration was as high as 1,000 ppm, and F=10 L/min, the toluene removal efficiency remained as high as 80% in the two-stage system using T_5S_4 as the fluidizing media. The toluene equilibrium removal efficiency was maintained in the 6-hr experimental time.

CONCLUSIONS

TiO_2/SiO_2 was prepared by the silica gel doping sol-gel method and characterized. EDS/SEM analyses indicate a flaky TiO_2 coated spherical silica gel structure. The as-prepared TiO_2/SiO_2 particles were used as the fluidizing media in a staged fluidized bed photoreactor. A slug fluidized bed allows good contact between TiO_2/SiO_2 particles and toluene molecules, and the large bubbles in the bed allow deep light penetration. Toluene is thus successfully being continuously degraded in the fluidized bed photoreactor.

The apparent reaction orders are 0.4-0.5 for single-stage reactors and 0.7 for two-stage reactors, respectively. The dual effects of the gas residence time and the flow regimes causes the highest equilibrium toluene removal efficiency to be at F=10 L/min when using T_3S_4 or T_5S_4 as the fluidizing media and at F=15 L/min when using T_9S_4 as the fluidizing media. The highest toluene removal efficiency of 87% was obtained in the two-stage system using T_5S_4 as the fluidizing media when the inlet toluene concentration is 300 ppm and F=10 L/min. When the inlet toluene concentration is as high as 1,000 ppm and F=10 L/min, the toluene equilibrium removal efficiency remains as high as 80% in the two-stage system using T_5S_4 as the fluidizing media. A rapid, continuous, long operation time, high concentration VOC degradation system is developed.

ACKNOWLEDGEMENTS

The authors are grateful for the financial support from the Ministry of Science and Technology, Taiwan (MOST 103-2221-E-182-068; MOST 104-2221-E-182-060-MY2) and Chang Gung Memorial Hospital (BMRP 634).

REFERENCES

1. M. Fujihira, Y. Satoh and T. Osa, *Nature*, **293**, 206 (1981).
2. H. P. Kuo, C. T. Wu and R. C. Hsu, *Powder Technol.*, **195**, 50 (2009).
3. H. Nouri and A. Habibi-Yangjeh, *Adv. Powder Technol.*, **25**, 1016 (2014).
4. D. S. Selishchev, P. A. Kolinko and D. V. Kozlov, *J. Photochem. Photobiol. A-Chem.*, **229**, 11 (2012).
5. S. M. Lam, J. C. Sin and A. R. Mohamed, *Korean J. Chem. Eng.*, **27**, 1109 (2010).
6. A. Motamed Dashliborun, R. Sotudeh-Gharebagh, M. Hajaghazadeh, H. Kakooei and S. Afshar, *Chem. Eng. J.*, **226**, 59 (2013).
7. H. P. Kuo, C. T. Wu and R. C. Hsu, *Powder Technol.*, **210**, 225 (2011).
8. A. L. Linsebigler, G. Lu and J. T. Yates Jr., *Chem. Rev.*, **95**, 735 (1995).
9. J. Jeong, K. Sekiguchi and K. Sakamoto, *Chemosphere*, **57**, 663 (2004).
10. M. Tasbihi, U. Lavrencic Stangar, U. Černigoj, J. Jirkovsky, S. Bakardjieva and N. Novak Tušar, *Catal. Today*, **161**, 181 (2011).
11. N. Takeda, T. Torimoto, S. Sampath, S. Kuwabata and H. Yoneyama, *J. Phys. Chem.*, **99**, 9986 (1995).
12. S. Alijani, A. Z. Moghaddam, M. Vaez and J. Towfighi, *Korean J. Chem. Eng.*, **30**, 1855 (2013).
13. P. L. Yue and F. Khan, *Chem. Eng. Sci.*, **38**, 1893 (1983).
14. C. Si, J. Zhou, H. Gao and G. Liu, *Adv. Powder Technol.*, **24**, 295 (2013).
15. D. Geldart, *Gas fluidization technology*, Johnson Wiley & Sons, Chapter 1 (1986).
16. H. Tang, S. Chang, K. Wu, G. Tang, Y. Fu, Q. Liu and X. Yang, *RSC Adv.*, **6**, 63117 (2016).
17. K. S. W. Sing, D. H. Everett, R. A. W. Haul, L. Moscou, R. A. Pierotti, J. Rouquerol and T. Siemieniewska, *Pure Appl. Chem.*, **57**, 603 (1985).
18. Q. J. Xiang, K. L. Lv and J. G. Yu, *Appl. Catal., B*, **96**, 557 (2010).
19. Y. Lin, T. Wang and Y. Jin, *Powder Technol.*, **123**, 194 (2002).